DTIC FILE COPY

AD-A220 466

Experimental Determination of the Electric Field and Charge Distribution in Magnetically Insulated Ion Diodes*

Y. Maron[a]

M.D. Coleman, D.A. Hammer, and H.S. Peng[b]

Laboratory of Plasma Studies

Cornell University

Ithaca, New York 14853

LPS 366 March 1987

Accession For
NTIS GRA&I
DTIC TAB
Unannounced
Justification per ltr
By
Distribution/
Availability Codes
Dist | Avail and/or Special
A-1

DTIC COPY INSPECTED 4

DTIC ELECTE APR 13 1990 S D
Co E

DISTRIBUTION STATEMENT A
Approved for public release;
Distribution Unlimited

90 04 12 149

Experimental Determination of the Electric Field and Charge Distribution in Magnetically Insulated Ion Diodes*

Y. Maron[a]

M.D. Coleman, D.A. Hammer, and H.S. Peng[b]

Laboratory of Plasma Studies, Cornell University

Ithaca, New York 14853

We have measured the electric field distribution across the high voltage gap of a magnetically insulated intense ion beam diode by observing the Stark shift of line-emission from ions accelerating in the gap. The measured distribution yielded the time dependence of the actual diode gap. We observed rapid gap closure early in the pulse, resulting from expansion of the electric field-excluding electrode plasmas in the diode. This can contribute substantially to the previously observed ion current density enhancements over the values calculated based upon the mechanical diode gap. Assuming planar geometry the electric field distribution was used to determine the electron density across the diode gap. This was compared with one-dimensional Brillouin-flow model calculations using the *actual* acceleration gap. The electrons were observed to spread towards the anode beyond the region of the theoretical electron-sheath. The electron presence near the anode was further enhanced when a cathode vane was used. In addition, an increase in the total electron number in the gap relative to analytic theory was inferred. This serves to explain the enhancement of the measured ion current density over the one calculated using the *actual* diode gap that we observed for the configuration tested.

*Supported by DOE Contract #DE-AS08-81DP40139 and ONR Contract #N00014-82-K-2059.

[a]Also, Physics Department Weizmann Institute, Rehovot, Isreal

[b]Present address: Southwest Inst. of Nuclear Physics and Chemistry, P.O. Box 515, Chengdu, China.

I. INTRODUCTION

Crossed electric and magnetic fields have been applied in a variety of high power charged particle beam devices. The magnetic field may be externally applied or it may be produced by the large beam currents in the device. Examples are: 1) magnetically insulated ion diodes[1-3] for the generation of intense ion beams; 2) plasma erosion switches[4,5] for high current switching; 3) magnetrons[6] for the generation of high power microwave radiation; and 4) high power electron diodes[7]. A common feature of these devices is that electrons and ions (drawn from the cathode and the anode plasmas, respectively) are accelerated by electric fields $>$ 1 MV/cm which prevail in gaps of a few millimeters to a few centimeters width between the electric-field-excluding plasmas in the devices. While the ions (being little affected by the magnetic fields) move in the acceleration gap along nearly straight trajectories, electrons execute complicated gyrations and drifts.

In magnetically insulated ion diodes, a magnetic field is applied parallel to the electrodes in order to inhibit electron flow to the anode, thereby enhancing the ion generation efficiency of the diode relative to the few percent or less predicted by space charge limited flow calculations[2]. Equilibrium solutions[8-10] for the electron and ion flow yield the distribution of the electric potential and the charge density in the gap under the key assumption of one-dimensionality. However, the actual charge flow does not obey these solutions, probably due to the finite size of the diodes[11], the non-uniformity of both the value and the direction of the applied magnetic field[2,12], and non-uniformities of the plasmas in the diodes[13,14]. These problems are demonstrated by a substantial electron flow to the anode (which significantly reduces the diode efficiency and causes damage to the anode surface) in spite of strong magnetic insulation. Such non-ideal configurational effects may also result[13,15] in a considerable divergence of the ion beams, which imposes limitation on their use[16].

Measurements inside high power diodes are difficult to perform due to the small gap spacing and high voltage stress there. Previous to the measurements reported here, only the plasmas in the diodes have been observed. The high density plasma front motion has been monitored using interferometry[17-19], plasma density has been measured by spectral line-broadening[19,20], and cathode-plasma temperature has been inferred from line intensity ratios[19]. However, these observations yielded the density profile of only the relatively dense part of the electrode plasmas ($\gtrsim 10^{15}\text{cm}^{-3}$) rather than the boundaries of the electric-field-excluding plasmas in the diode. The actual diode gap (i.e., the distance between the zero electric field positions) throughout the pulse was, therefore, still unknown. Thus, although possible effects of electrode plasma expansion in diodes have been considered[17,21-23], measured ion current densities were usually compared to theoretically predicted values based on the *mechanical* (initially set) diode gap. On the other hand, the electron flow in the gap and the ion current density are very sensitive to the actual diode gap; hence a better determination of the latter is necessary. Furthermore, no investigation of the potential distribution in the acceleration gap (between the electrode plasmas) has been attempted prior to the work presented here.

The present study was motivated by a recent suggestion[24] that the electric field in the acceleration gap of a high power ion diode can be determined by measuring the Stark shift of line-emission from ions traversing the gap, as shown schematically in Fig. 1a. Observation of the spectral profile of specially selected ion emission lines at different distances x [see Fig. 1(a)] from the anode allows the electric field distribution $E(x)$ across the diode acceleration gap to be obtained. In this scheme, in which ion spontaneous emission is observed, the measurement integrates over the line of sight, and the line-emission (collected parallel to the electrodes) is Doppler broadened due to the transverse ion motion (parallel to the electrodes). The Doppler broadening can be canceled by the use of two photon Doppler-free absorption of tunable dye laser light to excite the ions[24], which would yield local measurements of the electric field. Here we report measurements of the electric

field distribution in the gap of a magnetically insulated diode by the spontaneous emission method. The ions are excited in the anode plasma and are observed while accelerating in the diode gap [Fig. 1(a)]. For each position x, the electric field $E(x)$, averaged over a plane parallel to the anode, was obtained as a function of time in one or two pulses of the intense ion beam source.

We have measured[25] the electric field distribution $E(x)$ for planar diode configurations and for a vaned-cathode configuration. The $E(x)$ distribution showed that the electric field-excluding anode plasma expanded rapidly early in the pulse, causing a gap reduction which considerably affected the ion current density. The determination of the actual (instantaneous) diode gap throughout the pulse allowed a comparison of measured $E(x)$ profiles and ion current densities with one-dimensional calculations[9] for a magnetically insulated diode which has the measured accelerating gap, voltage, and applied magnetic field. Furthermore, from the experimentally determined E(x) and charge distributions, it is possible to obtain the distributions of the electrostatic potential, ion density, and the electron density. The additional assumption of laminar ExB electron drift motion can then be used to obtain the distribution of the electron drift current in the diode gap. Finally, the total electron drift current can be compared with the diode electron current that is inferred from the measured total diode current minus the ion current obtained from Faraday cup measurements of the ion current density together with the active diode area. The inferred electron density distribution showed electron presence close to the anode beyond the region of the calculated electron-sheath. For the planar cathode configuration this phenomenon was associated, in certain cases, with a measured ion current density about twice the calculated one. For the vaned cathode configuration the electron migration towards the anode was more pronounced and was accompanied by an increase in the total electron number in the gap. The total electron drift current was about twice the calculated value. The extra electrons in the gap provide a qualitative explanation for our observed ion current density enhancement of 3-8 over the value calculated[9] using the *actual* diode gap.

II. EXPERIMENTAL SYSTEM

In order to obtain line-emission from ions traversing the gap, the ions must be excited in the anode plasma and the upper level of the transition must have a life-time about equal to the ion transit time in the gap (a few nanoseconds). If the lifetime is much longer, the emission in the gap may be too weak to obtain reasonable accuracy. Secondly, the Stark shift of the line-emission under the influence of electric fields in the range of interest must be sufficiently large that the Doppler broadening of the line which results from transverse ion velocities is not important[24]. Proton beam divergences of about 5° were measured outside the diode used for these experiments[26]. If such a divergence were present inside the diode the Doppler broadening of a visible line emitted in the transverse direction from ions produced in a 300 kV diode would be of the order of 1 Å. For a Stark shift to exceed this, line emission from a high-lying upper level of a light ion must be used. Alternatively, heavy ions can be accelerated in the gap[24] for which energy levels close to the ground level can also be sufficiently Stark shifted. Obviously, the shift must also be smaller than the spectral distance to nearby line-emission. An additional consideration is that the observed ions must be abundant in the anode plasma (which is composed mostly of protons in magnetically insulated diodes unless major effort is invested to avoid them[15]); the desired upper level must be sufficiently populated so that the small fraction of ions drawn from the plasma into the gap will provide sufficiently intense emission. Furthermore, the observed ions must be easily and reproducibly generated in the anode plasma. Finally, since the electric field is inferred from the measured line shift, the oscillator strengths of the relevant dipole transitions should be known relatively well. (The uncertainty in the calculation, however, only scales the inferred values of E, thus not affecting the distribution of $E(x)$). Hence, it may be advantageous to select an ion with one electron in the outer shell.

For our experiments we used the racetrack shaped planar magnetically insulated diode[26] which is illustrated in Figs. 1(b). The insulating magnetic field (B_z=5-8kG)

which inhibits the electron motion across the gap was produced by an external current through a single turn coil which also acted as the cathode. The dielectric-anode surface was made up of a 140×50×1.6 mm^3 polyethylene sheet (with the long dimension parallel to B_z) drilled with 1 mm diameter holes, 2.7 mm apart. The diode was powered by about a 400 kV, 80 ns pulse delivered by a 10 Ω transmission line mounted on the output of a 5Ω pulse forming line. Typical diode voltage and current waveforms are shown in Fig. 2.

A schematic diagram of the optical arrangement is shown in Fig. 1(c). Line-radiation emitted in the z direction from a surface parallel to the anode was directed by the mirror M to a lens L which focused it on the input slit of a λ-Minuteman 0.5 m spectrometer. Light was collected from a volume 14 cm long and 5 cm high as determined by the input slit length (4 mm) and the demagnification factor 12 of the lens L. The thickness of this volume in the x direction (i.e.-the spatial resolution) of 0.6 mm was similarly determined by the slit width of 50 μm. The spatial resolution was also checked by observing light from a point source placed in different regions of the diode viewed by the system.

Using the cylindrical lens CL [see Fig. 1(c)], the spectrometer output was magnified about 10 times to further disperse the spectrum. It was then directed onto an array of seven fiber bundles, each 10 mm high and 0.8 mm wide. The width of the spectral window observed by each fiber bundle was determined by the lens magnification and input slit width. The spectral resolution of the system for the 50 μm input slit was 0.7 Å. Each fiber bundle transmitted the light to a photomultiplier tube, the signal from which was recorded by an oscilloscope giving a temporal resolution of 8ns. Thus, seven points of a spectral line profile were obtained as a function of time in a single discharge.

For our measurements, we selected the Al^{++} ions produced in the anode plasma from an aluminum coating on the polyethylene anode which resulted from aluminum blown off the anode stalk due to electron bombardment. We used the radiative decay of the 4*d* level (20.6 eV) which is Stark shifted mainly due to interaction with the 4f level. The shift results in a red shifted radiative transition to the almost unshifted 4p level. We made

most of our measurements on the $4d_{\frac{5}{2}} \rightarrow 4p_{\frac{3}{2}}$ (4529.2 Å) line although the shift of the $4d_{\frac{3}{2}} \rightarrow 4p_{\frac{1}{2}}$ emission (4512.5 Å) was also observed. The electric field causes the $4d_{\frac{5}{2}}$ level to split into three shifted components. Further modification of the emission pattern results from the magnetic field (Zeeman effect). For most of our measurements, the entire line profile could be obtained on a single discharge using the seven channel fiber bundle array with 0.7 Å width per channel. However, when the electric field was $\geq$ 1.2 MV/cm, the shifted line profile was sufficiently broad that the complete profile had to be obtained on two successive shots.

We note that except for the first few discharges after the insertion of a new polyethylene anode sheet, the electric field derived from Al^{++} line-emission was reproducible to within 10% for more than a hundred discharges, thus allowing us to obtain the electric field distribution across the entire diode gap using the same diode set up.

The ion current density J_i was measured using negatively biased Faraday cups placed 17 cm from the anode. To determine the fraction of ions heavier than protons in the ion beam, we placed 2 μm thick polyethylene foil (which lets through only protons of at least 180 keV energy) in front of the cups. From such measurements and ion time of flight considerations we concluded that the non-protonic component of the ion beam was about 35%. From observed line-emission from the anode plasma we believe that this component is comprised mainly of singly and doubly charged ions of carbon, oxygen, nitrogen, and aluminum.

III. MEASUREMENTS

A. Line-shift measurements

For each diode configuration, we first observed line-emission from a position about 1 mm from the solid anode surface. This region is occupied by the electric-field-excluding anode plasma. The line emission from this region started about 15 ns, and reached a plateau about 35 ns, after the start of the diode voltage pulse (denoted here as t=0). A typical profile of the 4529 Å Al^{++} emission from the anode plasma is shown in Fig. 3(a) for t=70 ns. Each point represents the signal recorded by one fiber channel. The profile is unshifted, consistent with previous measurements[27] which showed a negligible shift for this line at our anode plasma density (less than 6×10^{15} cm^{-3} [20]). The observed line-width was determined by the system spectral resolution. Observations of the emission from the anode plasma were used to verify that the plasma provided no other line-emission close to the lines of interest.

The mirror M [see Fig. 1(c)] was then moved to observe ion emission from the acceleration gap. The light signal from the gap began coincident (within our temporal resolution) with the start of the light signal from the anode plasma, as expected from the short ion transit time in the gap. Also, it was a few hundred times smaller than that from the plasma on the electrodes. A profile of the red shifted 4529 Å line-emission from the gap is shown in Fig. 3(b). The signal at the zero-field wavelength (i.e., the signal from the fiber channel centered at 4529.2 Å) was probably due to the unshifted intense plasma light scattered into the detection system (when it was set to look into the acceleration gap). Indeed, by varying the position of the window through which the light was extracted from the vacuum chamber, and placing baffles in the vacuum chamber to block the electrode light, we found that almost the entire unshifted signal of the 4529 Å line initially observed from the gap was due to scattered electrode light. Therefore, the residual signal at 4529Å was ignored when the ion emission from the gap was unfolded to give the electric field. We note that at later times, when the anode plasma expanded far enough into the gap to be observed

by the optical system, the measured line-emission became unshifted and about 100 times more intense, as expected.

B. Unfolding the electric field

In order to determine the electric field from the measured shifted line spectral profile, we calculated the expected emission pattern along the magnetic field from an ion under perpendicular electric E_x and magnetic B_z fields. Both electric and magnetic dipole contributions to the shifts and splitting of the ion energy levels were taken into account. We considered only the n=4 levels, since the interactions of the $4d$ and the $4p$ levels with levels of $n \neq 4$ have negligible effect. For the oscillator strengths we used values calculated by Cowan[28]. For B_z, we used the value of the externally applied magnetic field. This is justified since, firstly, the variation of the magnetic field in our low current diode due to diamagnetic effects is small[8-10]. Secondly, the magnetic field is assumed to totally penetrate the electrode plasmas based upon the field penetration time scale being short compared to the pulse length (determined using resistivities of the anode and the cathode plasmas calculated from the observed plasma conditions[17,19]). Furthermore, the calculated emission pattern was not sensitive to the value of B_z in the range 0-10 kG once Doppler broadening was included in each component of the shifted and split line.

In the calculation of the predicted spectral line profiles, each component of the $4d_{\frac{5}{2}} \rightarrow 4p_{\frac{3}{2}}$ emission was broadened to account for the Doppler broadening due to the ion transverse velocities. The Doppler broadening of the 4529 Å line was inferred from our measured[29] Doppler broadening of the 3602 Å Al^{++} line. The latter line is not shifted by the electric field; thus its broadening (FWHM $\sim$ 1 Å) was used to obtain the Al^{++} ions transverse velocities[29]. The Doppler broadening of the shifted pattern components had a negligible effect on the fit of the calculated pattern to the observed one because the broadening does not alter the average shift of the pattern. (The effect of the system spectral resolution was even smaller than that of the Doppler broadening). Examples of

calculated line profiles as seen by our spectral system for three values of E_x for B_z=0 are shown in Fig. 4.

The electric field was inferred from a least squares fit of the calculated emission patterns for a range of E_x (0.4-1.5 MV/cm) to the measured points of the emission spectral distribution. Since this analysis assumed a single value of the electric field, it gives, for each position, x, the mean electric field E over the gap region observed by the collection optics.

C. Tests of the measurement method

We observed line-emission from the gap which should not be measurably shifted by our electric fields. These lines were Al^{++} 5722 Å, Al^{++} 3602 Å, and C^{++} 4647 Å, all of which were unshifted. In addition, we observed the shift of the other transition from the Al^{++} 4*d* level i.e., the Al^{++} 4512 Å line ($4d_{3/2} \rightarrow 4p_{1/2}$). This line-emission must also be red shifted and, since the shift is determined by the 4f-4d oscillator strength, as is the case for the 4529 Å line, it should yield the same value for the electric field as that inferred from the 4529 Å(with no dependence on the specific value used for the oscillator strength). Indeed, the measured shift of these two lines yielded the same electric fields well within the measurement accuracy.

IV. RESULTS

The electric field profile $E(x)$ was measured for two types of cathodes. The first type (called here the "planar cathode") is a planar cathode made of a slotted aluminum plate with an ion transmissivity of 58%. In the second type (called here the "vaned cathode"), a 14-cm-long thin stainless-steel vane was connected to the cathode [see Fig. 1(b)], opposite the top of the dielectric-anode, parallel to the magnetic field lines (the electrons in the gap ExB drifted downward). The vane projected 3.5 mm into the gap. Electrons originating from the tip of the vane and ExB drifting in the gap are often described as forming a "virtual cathode" over a plane parallel to the anode and including the vane tip[15]. The purpose for using this configuration was to examine whether indeed such a virtual cathode is formed and if it screens out the electric field from the region between the cathode plasma and the vane tip. For this configuration we also attempted to check whether the formation of the virtual cathode is responsible for the observed enhancement in the ion current density. Using vaned cathodes, we observed an ion current density, about 120 A/cm^2, which is significantly larger than that expected based upon the diode voltage, the applied magnetic field and the mechanical spacing. The anode surface-to-cathode surface spacing yields a predicted current density of about 8 A/cm^2, while the anode surface-to-vane tip distance gives about 20 A/cm^2. This discrepancy will be discussed in Section V.

Using a planar cathode we measured the profiles $E(x)$ for three sets of parameters: B=8.0 kG, d_o=0.75 cm; B=6.7 kG, d_o=0.75 cm; and B=8.4 kG, d_o=0.65 cm, where B and d_o are the applied magnetic field and the mechanical A-K gap, respectively. The diode voltage V_d was measured with a capacitive monitor located at the output of the power feed to the diode, the signal from which was corrected for the inductive voltage drop between the monitor location and the diode gap.

Profiles of $E(x)$ for B=8.0 kG and d_o=0.75 cm are given in Fig. 5 at three times after the start of the diode voltage pulse: t=35, 55, 75 ns. Also shown is a profile for the same d_o but for B=6.7 kG. The measurement error indicated in the figures is dominated by the fluctuations of the PM-tube signals resulting from the weak ion emission from the diode gap. Some uncertainty in the inferred electric field was also due to the limited spectral resolution of the system (determined by the number of the fiber channels used to observe the shifted pattern).

As indicated by the error bars, the smallest measurable value for the electric field was 0.4 MV/cm, observed near the cathode and the anode plasmas. The diode regions between each of these two points and the closest electrode are occupied by the diode plasmas from which intense and unshifted line-emission was observed. An upper limit for the actual diode acceleration gap d (i.e., the distance between the position x_a on the anode side and the position x_b on the cathode side at which the electric field vanishes) is obtained from the distance between the positions at which anode and cathode plasmas are observed as indicated by intense line emission. A lower limit is determined from the distance between the positions on the two sides at which an electric field certainly larger than zero (i.e., > 0.4 MV/cm) is measured. These limits determine an uncertainty of $\pm$0.075 cm in inferring the actual diode gap d as a function of time from the measured $E(x)$ profiles. The diode voltage V can then be obtained from the integration $\int_o^{d_o} E(x)dx$. This gives 374, 367, 260, and 288 kV for the profiles in Figs. 5(a), 5(b), 5(c), and 5(d), respectively. These numbers should be compared to the instantaneous capacitive monitor values V_d, which are: 355, 355, 306, and 300 kV, respectively. V and V_d agree to within 15%, which is within experimental error for this pair of quantities (most of which is in the $E(x)$ measurement).

The electric field distributions given in Fig. 5 show that the field-excluding anode plasma expanded about 3 mm off the solid anode surface during the first 35 ns of the pulse, then expanded much slower (0.5 mm or less) between 35 and 75 ns. To determine the anode-plasma expansion velocity during the first period, the formation time of the

anode plasma must be known. Assuming that the plasma was formed at the solid anode surface at the start of the diode voltage pulse (t=0) or at the start of the Al^{++} line-emission near the anode surface (t≈15 ns) determines lower and upper limits, respectively, for the axial velocity of the electric field-excluding plasma. Accounting also for the measurement spatial resolution this yields a range of 5-15 cm/μs. Similar velocities were deduced from the observation of C^{++} line-emission.

For the vaned cathode configuration, we measured $E(x)$ for d_o=1 cm between the anode and the planar cathode and B=6.6 kG. Our optical system could not observe light from the top of the diode which ensured that no light from plasma produced at the vane tip could be detected. Figure 6 shows $E(x)$ profiles for t=35 and 45 ns. A strong electric field is present at positions between the planar solid cathode and the vane tip. The electric field vanishes only at the cathode plasma as in the cases of the planar cathode configurations. Thus, the virtual cathode formed by electrons emitted from the vane tip does not cause the electric field to abruptly drop to zero at the x position of the vane tip. This is consistent with 2D simulation results by Desjarlais and Sudan[30]. Note that the anode plasma expands about 3 mm during the first 35 ns of the pulse for the vaned cathode configuration, as for the planar cathode configuration.

V. DATA ANALYSIS

A. Electron Density Distribution

We analyze our measurements assuming one-dimensional geometry. We also assume that the electric field profile $E(x)$ is constant over a period equal to the ion transit time in the gap since no significant variation of the electric field could have been observed on this time scale with the oscilloscope used. For each time instant we normalize our $E(x)$ data points to give $\int_o^{d_o} E(x)dx = V_d$. We then draw smooth curves through the normalized $E(x)$ points, as shown in Figs. 7 and 8 for the data sets given in Figs. 5 and 6, respectively. Here we note that the electron density is determined by the local derivative of these curves. Therefore, since the curves are subjectively drawn, the electron-density distributions which we present from them should be regarded only as approximations. Later on we will discuss a quantitative analysis in which no use of these curves is made and for which error bars can be assigned.

We now compare our results to calculations based on the one-dimensional relativistic Brillouin-flow model[9] analyzed by Antonsen and Ott. We calculate the $E(x)$ profiles for each time instant using the instantaneous diode voltage V_d and the actual instantaneous diode gap d (determined as explained in Sec. IV). We use the applied magnetic field B_z for the magnetic field in the gap, as discussed in Sec. IIIB. Calculated $E(x)$ profiles are shown in Figs. 7 and 8. There is a noticeable tendency for the experimentally determined electric field to be higher than the calculated one in the region close to the anode. The difference is enough to be beyond the error bars of the measurement for the vaned-cathode configuration (Fig. 8). The difference between the measured and the calculated $E(x)$ profiles can occur if electrons are present close to the anode, unlike the model prediction of an electron-sheath confined near the cathode. (Notice that the maximum measured E-field is close to the anode while the boundary of the theoretical electron sheath is the point of maximum calculated E.) This can be demonstrated quantitatively by calculating the electron density profile $n_e(x)$ from the $E(x)$ profiles. To this end, we obtain the

potential profile $\varphi(x)$ across the gap, $\varphi(x) = V_d - \int_o^x E(x)dx$, from which the ion velocity profile can be determined:

$$v_i(x) = (2e(V_d - \varphi(x))/m_i)^{1/2},$$

where e is the ion charge, m_i is the ion mass, and $v_i(0)$=0. From $v_i(x)$ we obtain the ion density $n_i(x) = J_i/ev_i(x)$ using the measured ion current density J_i. To determine $n_i(x)$ from J_i we estimated that the beam non-protonic component has an average charge e and mass 10 m_p, where e and m_p are the electron charge and the proton mass, respectively (in keeping with the discussion in Sec. II). The uncertainty in this estimate does not affect the conclusions drawn below. A differentiation of the curve assumed for $E(x)$ can now be used to yield the electron density profile:

$$n_e(x) = n_i(x) - 5.53 \cdot 10^{11} \frac{dE}{dx}, \tag{1}$$

where $n_i(x)$ and $n_e(x)$ are expressed in cm^{-3} and $\frac{dE}{dx}$ is in $\mathrm{MV/cm}^2$. The profiles $n_e(x)$ thus obtained are compared in Figs. 9 and 10 to the calculated[9] ones for the measured electric field profiles shown in Figs. 7 and 8, respectively. This comparison shows the tendency of the electron cloud in the diode gap not to be confined to a relatively narrow region near the cathode as the Brillouin-flow model requires. The enhanced electron presence outside the theoretical electron-sheath region is seen more clearly for the vaned-cathode configuration (Fig. 10). Also, the spatial spread of the electron cloud towards the anode in the vaned-cathode case is significantly larger than the spatial resolution of our system. Evidently, the vane tip emits electrons which provide the electrons near the anode, as will be further discussed shortly.

Diffusion of electrons toward the anode from the cathode sheath has been treated theoretically[31,32,14]. Mouthaan and Susskind[31] suggested that electron transport across the magnetic field in a smooth-bore magnetron occurs due to the random fluctuations of the fields (brought about by a presumed instability in the electron flow) which cause the

electron positions to become a random function of time. On this basis they obtained spatial distributions (falling off towards the anode) of the electron charge and current density across the gap (no ion presence was assumed). Poukey and collaborators[32] suggested electron migration towards the anode due to the presence of an electric field E_y in the electron-drift direction that reduces the energy of the electron distribution. A significant electron pile-up near the anode was deduced for E_y about 10% of the vacuum E_x field. Desjarlais and Sudan[14] showed that small perturbations of the potential may bring about stochastic transport of electrons in the gap, leading to electron convection to the anode. They also pointed out the large sensitivity of the electron trajectories to small perturbations for equilibria near the Brillouin-flow state.

For a quantitative analysis which is much less dependent on the assumed $E(x)$ curves we proceed as follows. We define the total electron number $N_e(x) = \int_x^{x_c} n_e(x)dx$ per cm^2 between the cathode plasma boundary position x_c and a position x in the gap, given by:

$$N_e(x) = 5.53 \cdot 10^{11} E(x) + N_i(x), \tag{2}$$

where $N_i(x)$ is the total ion number per cm^2 between x_c and x, and $E(x)$ is expressed in MV/cm. A lower limit N_g for the total electron population per cm^2 in the diode gap is given by $N_e(x_1)$, where x_1 is the smallest x (i.e., closest to the anode) at which an electric field > 0 is measured. [For instance, x_1=0.35 cm and $E(x_1)$=0.95 MV/cm for the profile shown in Fig. 5(a).] The electron population in the region $x < x_1$ cannot be inferred from our data due to the large error in the electric field measurement very close to the anode plasma and the rapid rise of the ion density there. The total number of ions in the region $x > x_1$ can be determined relatively accurately since the ion density in this region changes relatively slowly, being within a factor of 3 of the fully-accelerated-ion density at the cathode. This is because the ions at the point x_1 have already accelerated to an energy of a few tens of keV. We will shortly return to the error bars of the various inferred parameters.

We now use the theoretical model[9] to calculate the electron-sheath thickness s and the total electron number N_{th} per cm^2 in the sheath (i.e., the theoretical number in the entire gap) as a function of time. In addition, we obtain, using Eq. 2, the experimental electron number N_s per cm^2 in a slab of thickness s adjacent to the cathode plasma i.e., $N_s = N_e(x_2)$ where $x_2 = x_c - s$. We define $\alpha = N_g/N_{th}$ and $\beta = N_g/N_s$. $\alpha - 1$ is a lower limit for the fractional difference between the total experimental electron number in the gap and the calculated one. $\beta - 1$ is the ratio of the number of electrons in the gap which reside outside the theoretical sheath region to the number of electrons within the sheath region. Assuming the ion current is space charge limited, one expects[32,33] that for the cases for which both α and β are larger than unity, the measured ion current density would be larger than the theoretical one. The theoretical ion current density J_{ith} is obtained from the value given by the model[9] (for the actual diode gap d) by assuming that the ion beam is comprised of 65% protons and 35% singly charged ions of mass $10m_p$, as mentioned above.

Table I lists the experimental parameters, the experimentally determined diode gap d, the calculated sheath thickness s and the calculated total electron number in the gap N_{th}, the inferred electron number N_s in the theoretical sheath region, the inferred electron number N_g in the entire diode gap, and the corresponding ion numbers in these regions (N_{si} and N_{gi}, respectively), at a few times for the three planar cathode configurations and the vaned-cathode configuration. Also given are the ratios α and β defined above, the actual ratio B/B_* of the applied magnetic field to the critical magnetic field[34] (B_* is determined using the actual diode gap d), the measured ion current density J_i, and the ratio J_i/J_{ith}. Figure 11 shows J_i/J_{ith} as a function of α and β using all the cases listed in Table I. In spite of the large error bars the results show that for most of the planar cathode cases, α and β are close to unity. This implies that for the planar configuration, the measured ion current density should tend to agree with the calculated value[34]. Indeed, for most of the planar cathode cases studied, the ratio J_i/J_{ith} based upon the actual diode

gap is close to 1. The cases for which α and β seem to be relatively large are the cases numbered 6 and 9 in Table I (see the points marked 6 and 9 in Fig. 11). The results for these two cases suggest, that for a relatively low magnetic field or a narrow planar gap, respectively, large electron population and electron migration towards the anode can occur late in the pulse (t=75 ns). The corresponding enhancement J_i/J_{ith} may be about 2, as shown in the figure.

Markedly larger values for α and β are obtained for the vaned-cathode configuration. The total electron number in the gap is more than twice the calculated value ($\alpha \gtrsim 2$) and the excess electrons reside mainly outside the region of the theoretical electron-sheath ($\beta \sim 2$). For this diode configuration a relatively large enhancement of the ion current density was observed, $J_i/J_{ith} \sim$ 3-8, as shown in Fig. 11. Such an enhancement evidently results from the electron accumulation near the anode, as discussed above.

The relatively large electron population close to the anode ($\beta \gtrsim 2$) in the vaned cathode cases can be reasonably understood since the vane-tip projects farther than the zero electric field position x_c on the cathode side. Electrons emitted from the vane tip approach the anode plasma since the actual B/B_*, using the distance between the vane-tip and the anode plasma is about 1. These electrons ExB drift over the entire anode area, thus suppressing the electron population in the theoretical sheath region. However, at the x position of the vane tip, they are not numerous enough to zero the electric field. Electrons emitted from the cathode plasma presumably contribute very little to the electron presence near the anode since the B/B_* for the distance between the anode and the cathode plasmas, for the vaned cathode configuration, is even larger than those for the planar cathode configurations (see the values of d in Table I). The inferred values of α ($\gtrsim 2$) for the vaned configuration implies that this phenomenon also results in an enhanced electron accumulation in the diode gap. The enhancement in the ion current density (with respect to the planar cathode configurations and to the theoretical solution) results from the increase in the electron population in the gap and the electron presence near the anode rather than from the

formation of a true virtual cathode (surface beyond which E=0) at the plane of the vane tip as previously[15] described. The possibility of an enhancement of the ion current due to electron accumulation in the diode gap has been considered previously[32].

We would now like to discuss the error bars indicated in Fig. 11 which were estimated by considering the errors due to variety of sources. The error in the determination of the actual diode gap d dominates the uncertainty in s, $N_{th}, B/B_*, \alpha = N_g/N_{th}$, and J_i/J_{ith}. This results from the great sensitivity of the calculated total electron number in the gap N_{th} (and the calculated ion current density J_{ith}) to the diode gap. It emphasizes the need for an accurate measurement of the actual diode gap in order to understand the charge flow in high power diodes. We note, however, that an increase in the gap d decreases s, J_{ith}, and N_{th} (and increases B/B_*). Hence, the error bars in Fig. 11(a) indicate the range within which α and J_i/J_{ith} may change together and in the same direction. The errors in the measured J_i or in the heavy-ion component in the beam (the latter is used for the calculation of J_{ith}, see earlier) are much smaller than the error in J_{ith} which is caused by the uncertainty in d. The error in β results from the error in $E(x)$ and $N_i(x)$ which are used to infer N_g and N_e [see Eq. (2)]. The shape of $n_i(x)$ is obtained relatively accurately since $n_i(x)$ changes relatively slowly in the region $x > x_1$ and it is dependent on $\varphi(x)$ which is obtained by an integration of the data points. Thus, the error in $N_i(x)$ (which is obtained by an integration of $n_i(x)$) is mainly due to the error in the measured J_i. In determining $N_i(x)$ the inferred zero-field point x_c at the cathode side was used. However, the uncertainty in x_c modifies $N_i(x)$ only slightly, thus causing a negligible error in the calculated electron population N_g and N_e.

The ion current density is often compared to the space-charge-limited value. In Table I we compare J_i to the monopolar space-charge-limited value J_{ic} which corresponds to the measured diode gap d. For completeness we also give J_i/J_{ico}, where J_{ico} corresponds to the mechanical gap d_o. This ratio is usually given in discussions of intense ion beam diodes. For the vaned-cathode configuration we use the mechanical distance between the vane tip

and the anode, 0.65 cm, to determine J_{ico} (again in keeping with analyses in previous studies). We note here that the error in the relations between the ratios J_i/J_{ith}, J_i/J_{ic}, and J_i/J_{ico} is relatively small since the error in J_i is common to these ratios, and the errors in J_{ic} and J_{ith} are about the same (both are caused by the uncertainty in d).

As seen in the table, the enhancement J_i/J_{ic} is only a few tens of percent larger than J_i/J_{ith} since the enhancement J_{ith}/J_{ic} due to the magnetic insulation is 1.2-1.6 for our diode configurations. This results from the fact that the ratios B/B_*, even when calculated using the actual diode gap, are moderately large (the B/B_* for the vaned cathode configuration given in Table I is also calculated using the zero electric field position x_c). Thus, for the planar cathode configurations, the actual enhancement J_i/J_{ic} is generally below 2 (see Table I). For the vaned cathode configuration J_i/J_{ic} is larger (as J_i/J_{ith} is larger). The enhancement J_i/J_{ico} is obviously considerably larger than J_i/J_{ic}. Also, the relative difference between the J_i/J_{ico} values for the planar cathode configurations and those for the vaned cathode configuration is smaller than the corresponding difference for the J_i/J_{ic} values since the difference between the actual gap and the mechanical diode gap is smaller for the vaned cathode configuration.

We note here that in spite of the large ion current enhancement observed for the vaned-cathode configuration, the diode efficiency does not increase significantly (it remains near 25%) due to the increase in the electron current, as will be discussed in the next subsection. Thus, the vaned cathode allows diode operation at a lower impedance than that of the planar diode, but with the same efficiency.

B. Electron current distribution

Our data can be analyzed to give information about the distribution of the electron drift current across the diode gap. The electron drift velocity $V_y(x)$ was obtained by assuming a laminar electron flow (based on simulation results[35]) i.e., $V_y(x) = -cE(x)/B(x)$. The distribution of the magnetic field $B(x)$ was calculated (from the measured electric

field distribution $E(x)$ and the ion kinetic pressure across the gap) using the momentum balance equation given by Mendel[36]. The variation of the magnetic field in our diode is about 10% according to the model. Thus, the profile of the electron drift-velocity $\mid V_y(x) \mid = cE(x)/B(x)$ approximately follows that of $E(x)$, as shown, for example, in Figs. 12 and 13 for the profiles given in Fig. 7 and 8, respectively. Also shown in these figures are the inferred current density profiles $J_y(x) = \mid en_e(x)V_y(x) \mid$ of the drifting electrons and the theoretical[6] ones $J_{yth}(x) = en_{eth}(x)V_{yth}(x)$. As expected, these profiles show that for the vaned cathode configuration (Fig. 13) $J_y(x)$ spreads towards the anode more than for the planar cathode configuration.

In a similar manner to the analysis of the electron density distribution we can obtain quantitative information about the distribution of the drift-current density by calculating the total drift-current in the gap ($I_y = \int_{x_a}^{x_c} J_y(x)dx$) and the drift-current in the region of the theoretical electron-sheath ($I_{ys} = \int_{x_c-s}^{x_c} J_y(x)dx$). Both quantities are per unit anode length. We define the ratio $\gamma = I_y/I_{ys}$ (analogous to β in Sec. VA), where γ-1 gives the ratio between the electron current outside the theoretical electron-sheath region to that within the sheath region. The ratio γ is given in Table I and is plotted in Fig. 14. Although the error bars are large, γ is systematically larger for the vaned-cathode configuration. Its value (between 2 to 9) means that the fraction of the drift-current outside the theoretical-sheath region is between 50% and 90%, indicating substantial electron flow close to the anode.

The inferred total drift-current I_y is compared in Fig. 15 with the theoretical[9] drift current $I_{yth} = \int J_{yth}(x)dx$ in the electron-sheath (the ratio I_y/I_{yth} is analogous to α in Sec. VA). Also given in the figure is the diode electron current I_e per unit length of the diode, obtained by dividing the total diode electron current by the anode length. The total experimental diode electron current is inferred from subtraction of the total ion current (obtained from the Faraday cup measurements by assuming a uniformity of J_i over the entire anode area) from the measured total diode current. The error in I_e may

be large due to uncertainty in the actual length of the active anode area and to possible nonuniformity of J_i where the anode is "turned on". The error in I_{yth} is about +70,-50% which is due to the uncertainty in the actual diode gap d. The error in the experimental I_y is estimated to be about ±30%. The comparison suggests that for the planar cathode configurations (cases 1-9) the observed I_y is generally close to the predicted I_{yth}, while for the vaned cathode configuration (cases 10-13) it is larger. This results from the increased electron total population in the diode gap (with respect to the theoretical one) for the vaned configuration.

VI. SUMMARY AND DISCUSSION

We have measured the electric field distributions $E(x)$ across the acceleration gaps of magnetically insulated intense ion beam diodes by observing the Stark shift of ion line-emission. We have used planar cathode configurations and a vaned cathode configuration in a "racetrack" shaped magnetically insulated diode.

Our measurements revealed rapid gap closure early in the pulse, resulting mainly from the expansion of the surface-flashover-produced anode plasma, at a velocity in the range (5-15) cm/μs. Such a gap contraction (by about 3 mm at 35 ns into the diode voltage pulse) considerably affects the ion current density. Johnson and collaborators[37] have said that a plasma expansion velocity of 5 to 10 cm/μs throughout the voltage pulse was required to explain the temporal impedance decrease in their applied-B ion diodes. The early fast expansion of the anode plasma and its slower expansion later on in the pulse observed here are not explained as yet.

The determination of the instantaneous *actual* diode gap d allowed us to determine the actual ion current enhancement J_i/J_{ic} and to compare the measured $E(x)$ distributions, assuming planar geometry, with a one-dimensional solution for magnetically insulated gaps. This comparison showed that the measured electric field tends to be larger close to the anode and smaller close to the cathode than the one predicted by the Brillouin-flow model[9]. The $E(x)$ profiles together with the measured ion current densities were analyzed to study the ion and electron density distributions in the diode gap. This analysis showed that for the diode configurations used, the electron cloud in the gap is not confined to a narrow sheath near the cathode; rather it migrates towards the anode. The measured $E(x)$ profiles were also used to infer the distribution of the electron drift-velocity and the electron-drift current density $J_y(x)$ under the assumption of laminar E $\times$ B flow.

The enhanced electron presence near the anode may result from electron transport due to the effects on the drifting electrons of spatial nonuniformities (such as from nonuniform expansion of anode and cathode plasmas) or temporal fluctuations of the electric

field[31,32,34]. For the planar cathode configuration, the electron presence near the anode does not seem to result in a significant enhancement of the ion current over the one (J_{ith}) calculated[9] using the actual diode gap d. However, when the total electron number in the gap is larger than the calculated[9] value (see points 6 and 9 in Fig. 11), an enhancement $J_i/J_{ith} \sim 2$ may have been observed. This is expected[32,33] if the ion current is assumed to be space-charge-limited.

For the vaned-cathode configuration the increase of the total electron number over the theoretical value (by a factor $\gtrsim$2) and the electron presence near the anode are more pronounced (about half of the electrons in the gap reside outside the theoretical sheath region). The electron accumulation near the anode is associated with an enhancement of about 3-8 of the measured ion current J_i over the one (J_{ith}) predicted by a one-dimensional Brillouin-flow-model solutions[9] of a magnetically-insulated configuration. While we believe that the relative comparison between the (J_i/J_{ith}) values for the planar and the vaned cathode configurations is valid, the absolute value of J_i/J_{ith} has to be treated cautiously since, as mentioned above, J_i is obtained with Faraday cups which view a small area of the anode.

The electrons near the anode presumably are emitted from the vane and ExB drift to cover the whole anode surface. However, they are insufficient in number to eliminate the electric field behind the vane tip, and emission from the cathode plasma evidentally occurs. We attempted to examine whether considerable electron accumulation near the anode would also occur in a planar cathode configuration with d_o=0.65 cm (the same as the vane-tip-to-solid anode distance in the vaned cathode configuration) and about the same magnetic field as that for the vaned cathode configuration. In those experiments a considerable decrease in the diode impedance occurred. Keeping d_o to be 0.65 cm and increasing B to 8.4 kG (see lines 7-9 in Table I) prevented the impedance collapse. However, the electron presence near the anode was less pronounced than in the vaned-cathode configuration (α and β were not as large - see Table I), although a moderate

increase in the electron population seems to have occurred at t=75 ns [see the points marked g in Figs. 11(a) and 11(b)]. The implication of this result is that, for the same diode efficiency, a vaned cathode yields higher ion currents than a planar one (i.e., it allows diode operation at lower impedance while maintaining the efficiency). Increasing the ion current with a planar cathode by applying a weaker magnetic field results in a reduction of the diode efficiency.

For both the vaned and the planar cathode configurations the enhancement J_i/J_{ic} of the ion current density with respect to the actual space-charge-limited value (calculated using the measured diode gap d) is a few tens of percent larger than J_i/J_{ith} (see Table I), since J_{ith} is only 20 to 60% larger than J_{ic} (due to the electrons in the theoretical cathode sheath). Calculating the ion current enhancement J_i/J_{ico} (using the mechanical gap d_o) gives, for our diode configurations, values larger by 2-4 than the actual values J_i/J_{ic}. Furthermore, the ratio J_{ic}/J_{ico} varies for different diode configurations. Thus, in studying ion diode operation, one has to be cautious if one compares values of the enhancement J_i/J_{ico} for different configurations.

The difference between the inferred drift current density $J_y(x)$ and the calculated profile $J_{yth}(x)$ is also much more pronounced for the vaned cathode configuration. $J_y(x)$ spreads considerably towards the anode (see the relatively large values of γ in Fig. 14 for the vaned cathode configuration) and the total experimental drift current I_y is about twice the calculated value I_{yth} (see cases 10-13 in Fig. 15). For higher intensity diodes, such an increase in the electron drift current and its broad distribution across the gap would result in strong diamagnetic effects which would considerably affect the distribution of the electron density and the ion current density, as discussed in refs. 22 and 23. In addition, this may cause an increase of the diamagnetic currents in the anode plasma which may affect the plasma properties.

We may compare our results to those obtained by Slutz and collaborators[23] from a computer simulation of a virtual cathode configuration operating at 1.5-3 MeV in which

no plasma expansion was taken into account. In this study, an annular cathode geometry was assumed, with the distance between the cathode blade and the anode corresponding to a B/B_* close to 1. This is similar to the B/B_* for our vaned-cathode configuration if the distance between the vane-tip and anode-plasma front is used. The simulation reveals an enhancement factor of 16 for the ion current density over the space-charge-limited value. The authors believe that about a factor 4 of this enhancement results from a substantial motion of the virtual cathode towards the anode due to diamagnetic effects (which are absent in our relatively low-current diode). One would expect, therefore, that in virtual-cathode diodes which utilize surface-flashover anode plasmas and in which diamagnetic effects are also significant, the early gap closure would contribute to producing large enhancements of the ion current density (with respect to J_{ico}). This may serve to explain the enhancement factors of up to 40 reported by Miller[22] on the basis of accumulated data from Proto I, Proto II, and PBFA-I.

We believe that our diagnostic tool can be utilized to obtain detailed information about the charge flow in various high-power, high voltage devices especially if the spatial resolution and the accuracy in measuring $E(x)$ are improved. Better measurement accuracy can be obtained mainly by increasing the intensity of the observed line-emission from the gap. Either the concentration of the ion species being observed must be larger or a line with stronger emission must be selected. For diodes powered by higher voltage pulses, the light signal can be larger due to the higher ion current density. Also, due to the quadratic dependence of the shift on E, the higher the electric field in the diode, the easier is the selection of lines suitable for these measurements, since low-lying ion energy level will be sufficiently Stark shifted. Observing emission from low-lying levels would also result in a more intense emission from the gap. Once more intense emission in a line of interest is achieved, it will be possible to use a larger number of fiber channels for observing the spectral emission profile. The resulting improvement in the spectral resolution would increase the accuracy in determining the electric field from the shifted pattern. Finally,

if the ion beam divergence does not increase for higher electric fields, then the Doppler broadening effect for higher voltage diodes would be much smaller, since the Stark shift increases quadratically with $E(x)$ while the ion transverse velocities will increase with the square root of the voltage. For higher electric fields suitable ion lines may be: Al^{++} 3713Å for E about 2 MV/cm, Al^{++} 5722 Å for E about 4 MV/cm, C^{++} 4647 Å for E about 4 MV/cm, and Al^{++} 3602 Å for E about 5 MV/cm. We have observed these lines in our diode gap[25,30] but they were shifted very little under our electric fields.

Due to the great sensitivity of the charged particle flow in the diode to the actual diode gap, the uncertainties in our data analysis were dominated by the uncertainty ($\pm$0.75 mm) in determining the actual diode gap d (i.e., the zero-field points in the gap). Thus, an improvement of the spatial resolution which could also come from more intense line emission, will significantly improve the comparison of future results with theoretical treatments[8-10].

Finally, intense line-emission will allow local measurements (perpendicular to the acceleration direction) to be made since specially selected ions can be "seeded" in a localized area of the anode for observation by our method. Furthermore, a better spatial resolution in the axial direction can be obtained by observing a narrower region of the gap. Improvement in the spectral resolution will allow measurements of smaller electric fields as long as the Doppler broadening does not exceed the Stark shift, thus again increasing the accuracy in determining d. Employing the laser-induced-fluorescence technique with a geometry as previously suggested[24], is expected to result in better spectral resolution as well as satisfactory spatial resolution in all directions. We believe that the improved measurements that we are suggesting will contribute substantially to achieving an understanding of the details of electron flow and their dependence on diode geometry in general and on the nonuniformities in the electrode plasmas in particular.

ACKNOWLEDGMENT

One of the authors (Y.M.) wishes to thank C. Mendel for valuable suggestions. The authors are grateful to R.N. Sudan and M. Desjarlais for stimulating discussions and to E. Elias for assistance in the data analysis. Y. Maron is the incumbent of the Reiter Family Chair at the Weizmann Institute. This research was supported by U.S. DOE contract # DE-AS08-81DP40139 and U.S. ONR contract # N00014-82-2059.

REFERENCES

1. P.L. Dreike, C. Eichenberger, S. Humphries, and R.N. Sudan, J. Appl. Phys. **47**, 85 (1976).
2. S. Humphries, Jr., Nuclear Fusion **20**, 1549 (1980), provides a review of intense ion beam generation.
3. G. Yonas, in *Proc. of IAEA Meeting on Advances in Inertial Confinement Fusion Research*, edited by C. Yamanaka (Kobe, Japan, 1983), p. 307.
4. See, for example, R.A. Meger, *Fifth Int. Conf. on High-Power Particle Beams*, (San Francisco, Calif. 1983), p. 330, and references therein.
5. P. Ottinger, S.A. Goldstein, and R.A. Merger, J. Appl. Phys. **56**, 774 (1984).
6. T.J. Orzechowski and G. Bekefi, Phys. Fluids **19**, 43 (1976), and **22**, 978 (1979).
7. See, for example, R.B. Miller, **Intense Charged Particle Beams** (Plenum Press, New York, 1982) Ch. 2, and references therein.
8. R.N. Sudan and R.V. Lovelace, Phys. Rev. Lett. **31**, 1174 (1973).
9. T.M. Antonsen and E. Ott, Phys. Fluids **19**, 52 (1976).
10. K.D. Bergeron, Appl. Phys. Lett. **28**, 306 (1976).
11. R.N. Sudan, in *Proc. 4th Int. Top Conf. On High-Power Electron and Ion Beam Research and Technology* (Palaiseau, France, 1981), p. 389.
12. J.B. Greenly and H.S. Peng, private communication.
13. Y. Maron, Phys. Fluids **27**, 285 (1984); Y. Maron and C. Litwin, to be published in Phys. Fluids.
14. M. Desjarlais and R.N. Sudan, Phys. Fluids **29**, 1245 (1986).
15. J.M. Neri, Ph.D. Thesis, Cornell University, 1982.
16. Craig L. Olsen, Laser and Particle Beams **2**, 255 (1984); G. Yonas, **Plasma Physics and Controlled Nuclear Fusion Research 1982**, Vol II (IAEA, Vienna, 1983), p. 353, and references therein.
17. D.J. Johnson, E.J.T. Burns, J.P. Quintenz, K.W. Bieg, A.V. Farnsworth, Jr., L.P.

Mix, and M.A. Palmer, J. Appl. Phys. **52**, 168 (1981).

18. J.E. Maenchen, F.C. Young, R. Stringfield, S.J. Stephanakis, D. Mosher, Shyke A. Goldstein, R.D. Genuario, and G. Cooperstein, J. Appl. Phys. **54**, 89 (1983).
19. D. Hinshelwood, NRL Memo. Report 5492 (1985).
20. R. Pal and D.A. Hammer, Phys. Rev. Lett. **50**, 732 (1983).
21. S. Humphries, Jr., J.R. Freeman, J.B. Greenly, G.W. Kuswa, C.W. Mendel, J.W. Poukey and D.M. Woodall, J. Appl. Phys. **51**, 1876 (1980).
22. P.A. Miller, J. Appl. Phys. **57**, 1473 (1985).
23. S.A. Slutz, D.B. Seidel and R.S. Coats, J. Appl. Phys. **59**, 11 (1986).
24. Y. Maron and C. Litwin, J. Appl. Phys. **54**, 2086 (1983).
25. Y. Maron, M.D. Coleman, D.A. Hammer, and H.S. Peng, Phys. Rev. Lett. **57**, 699 (1986).
26. J. Maenchen, L. Wiley, S. Humphries, Jr., E. Peleg, R.N. Sudan, and D.A. Hammer, Phys. Fluids **22**, 555 (1979).
27. M.A. Mazing and N.A. Vrublevskaya, Optics and Spectroscopy **16**, 6 (1984)
28. R.D. Cowan, private communication.
29. Y. Maron, M.D. Coleman, D.A. Hammer, and H.S. Peng, in J. Appl. Phys. **61**, in press (1987).
30. M.P. Desjarlais and R.N. Sudan, private communication.
31. K. Mouthaan and C. Susskind, J. Appl. Phys. **37**, 2598 (1966).
32. J.W. Poukey, S. Humphries, Jr., and T.R. Lockner, Phys. Fluids **25**, 1471 (1982).
33. Shyke A. Goldstein and R.Lee, Phys. Rev. Lett. **35**, 1079 (1975).
34. R.V. Lovelace and E. Ott, Phys. Fluids **17**, 1263 (1974); A.W. Hull, Phys. Rev. **18**, 31 (1921).
35. D.B. Seidel, S.A. Slutz, and C.W. Mendel, private communication.
36. Mendel, Jr., C.W., J. Appl. Phys. **50**, 3830 (1979); C.W. Mendel, Jr., D.B. Seidel, and S.E. Rosenthal, *Laser and Particle Beams* **1**, 311 (1983).

37. D.J. Johnson, G.W. Kuswa, A.V. Farnsworth, Jr., J.P. Quintenz, R.J., Leeper, E.J.T. Burns, and S. Humphries, Jr., Phys. Rev. Lett. **42**, 610 (1979); D.J. Johnson, P.L. Dreike, S.A. Slutz, R.J. Leeper, E.J.T. Burns, J.R. Freeman, T.A. Mehlhorn, and J.P. Quintenz, J. Appl. Phys. **54**, 2230 (1983).

TABLE I

The diode voltage V_d, actual measured diode gap d, theoretical electron-sheath thickness s and total electron number N_{th}, experimental electron numbers, N_g and N_s in the entire gap and in the theoretical sheath region, respectively (see Sec. VA), the corresponding ion numbers N_{gi} and N_{si}, and the ratios $\alpha = N_g/N_{th}$ and $\beta = N_g/N_s$. Also given are the measured ion current density J_i, the actual B/B_*, the actual ion current enhancements J_i/J_{ith} and J_i/J_{ic}, the ratio J_i/J_{ico}, and the ratio γ between the experimental total electron drift current in the diode gap to the current in the theoretical sheath region, for the three planar cathode configurations and the vaned-cathode configuration at 3 or 4 times during a pulse.

FIGURE CAPTIONS

Fig. 1: (a) Method for measuring the electric field E in the acceleration gap of a magnetically insulated diode. (b) An end view of the ion diode showing the location of the cathode vane and the anode ion emission region. (c) Schematic illustration of the planar magnetically insulated ion diode and the optical arrangement. The distance of the observation region from the anode is varied by moving the mirror M in the x direction.

Fig. 2: Typical inductively corrected diode voltage (monitored by a capacitive probe) and diode current waveforms.

Fig. 3: (a) Spectral profile of the $4d_{5/2} \rightarrow 4p_{3/2}$ Al^{++} emission from the anode plasma (x=0.15 cm) at t=70 ns. The zero-field wavelength is 4529.2 Å. The initial A-K gap (d_o) was 0.65 cm, the peak diode voltage was about 300 kV, and B was 8.4kG. The spectral window of each fiber channel was 0.67 Å. (b) Profile of the emission from the acceleration gap: x=0.375 cm and t=65 ns. The lines in (a) and (b) indicate the trend.

Fig. 4: Calculated spectral profiles for the $4d_{5/2} \rightarrow 4p_{3/2}$ Al^{++} emission for three electric fields with B=0. Each of the components of the shifted emission was assumed to be Gaussian-like with a FWHM of 1.3 Å due to Doppler broadening. The zero-field wavelength is 4529.2 Å.

Fig. 5: The measured electric field distribution $E(x)$ for a planar diode configuration with d_o=0.75 cm is shown at the three times 35, 55, and 75 ns in (a), (b), and (c) respectively. (d) The electric field profile for a similar configuration but with a different applied magnetic field B. The solid anode surface is at x=0 and the cathode surface is indicated by C. Each point is an average of two discharges.

Fig. 6: Measured $E(x)$ profiles at two times for a vaned-cathode configuration with d_o=1cm, peak diode voltage about 280 kV, and B=6.6 kG. The solid anode surface is at x=0 and the cathode is indicated by C. Each point is an average of two discharges. The vane projected 0.35 cm off the cathode surface, as indicated by the line l.

Fig. 7: The solid lines in (a), (b), (c), and (d) are simply smooth curves drawn through the data points (open circles) from Figs. 5 (a), (b), (c), and (d), respectively. The dashed lines are calculated[9] $E(x)$ profiles (see Sec. VA) using the instantaneous diode gap $d = x_c - x_a$, where x_a and x_c are the zero-field points on the anode and cathode sides, respectively.

Fig. 8: The same as Fig. 7 but for the data in Fig. 6 (vaned configuration).

Fig. 9: Electron density profiles $n_e(x)$ inferred from the $E(x)$ profiles in Fig. 7. Also shown are the corresponding Brillouin-flow[9] profiles calculated using the actual diode gap d.

Fig. 10: Electron density profiles inferred from the $E(x)$ profiles in Fig. 8 and the corresponding Brillouin-flow[9] profiles.

Fig. 11: The ion current density enhancement J_i/J_{ith} (with J_{ith} calculated[9] using the actual diode gap d) as a function of α and β for the cases listed in Table I. The circles belong to rows 10-13 (vaned-cathode configuration). The points marked by 6 and 9 correspond to rows 6 and 9 in Table I, respectively.

Fig. 12: Profiles of the electron drift velocity $\mid V_y(x) \mid$ and the drift current density $J_y(x)$ inferred from the $E(x)$ profiles in Fig. 7. Also shown are the corresponding theoretical[6] current densities $J_{yth}(x)$.

Fig. 13: Profiles of $\mid V_y(x) \mid$, $J_y(x)$, and $J_{yth}(x)$ for the cases in Fig. 8.

Fig. 14: The ratio $\gamma = I_y/I_{ys}$ for the cases listed in Table I. The numbers along the ordinate are the row numbers in the table. The circles correspond to rows 10-13 in Table I (vaned configuration).

Fig. 15: The total electron drift current I_y obtained from integration of $J_y(x)$ and the corresponding calculated total drift current I_{yth} for the cases listed in Table I. Also shown is the diode electron current I_e per unit anode length.

Table 1

No.	CONFIGURATION	t (ns)	V_d (kV)	d (cm)	s (cm)	N_{th} ($\frac{10^{11}}{cm^3}$)	N_g ($\frac{10^{11}}{cm^3}$)
1	Planar Cathode	35 ±5ns	356 ±10%	0.425 ±0.075	0.15 ±0.04	8.1 $^{+40\%}_{-20\%}$	7.4 ±15%
2	d_o = 0.75 cm B = 8.0 kG	55	355	0.425	0.15	8.1	8.4
3		75	306	0.375	0.14	8.2	8.3
4	Planar Cathode	35	310	0.425	0.18	7.6	7.9
5	d_o=0.75 cm B=6.7 kG	55	300	0.425	0.17	7.2	7.8
6		75	245	0.375	0.15	6.8	8.0
7	Planar Cathode	35	295	0.35	0.13	8.4	9.4
8	d_o=0.65 cm B = 8.4 kG	55	270	0.35	0.11	7.7	9.1
9		75	230	0.35	0.09	5.2	9.5
10	Vaned Cathode	35	260	0.475	0.13	4.7	13.9
11	d_o=1 cm B = 6.6 kG	45	260	0.475	0.13	4.7	13.5
12		55	245	0.475	0.12	4.3	12.8
13		65	230	0.475	0.12	4.0	12.3

TABLE I

The diode voltage V_d, actual measured diode gap d, theoretical electron-sheath thickness s and total electron number N_{th}, experimental electron numbers, N_g and N_s in the entire gap and in the theoretical sheath region, respectively (see Sec. VA), the corresponding ion numbers N_{gi} and N_{si}, and the ratios $\alpha = N_g/N_{th}$ and $\beta = N_g/N_s$. Also given are the measured ion current density J_i, the actual B/B_*, the actual ion current enhancements J_i/J_{ith} and J_i/J_{ic}, the ratio J_i/J_{ico}, and the ratio γ between the experimental total electron drift current in the diode gap to the current in the theoretical sheath region, for the three planar cathode configurations and the vaned-cathode configuration at 3 or 4 times during a pulse.

Table 1

NO.	CONFIGURATION	N_{gi} $(\frac{10^{11}}{cm^3})$	N_s $(\frac{10^{11}}{cm^3})$	N_{si} $(\frac{10^{11}}{cm^3})$	α	β	B/B_*
1	Planar Cathode	1.5	6.3	0.6	0.91	1.2	1.5
		±15%	±15%	±15%	+26% −50%	+42% −36%	±20%
2	d_o=0.75 cm B=8.0 kG	2.1	6.4	0.9	1.0	1.3	1.5
3		2.0	5.9	0.9	1.0	1.4	1.4
4	Planar Cathode	2.6	6.3	1.5	1.0	1.3	1.3
5	d_o=0.75 cm B=6.7 kG	2.8	5.8	1.4	1.1	1.3	1.4
6		3.5	6.5	2.0	1.2	1.2	1.4
7	Planar Cathode	2.7	7.1	1.5	1.1	1.3	1.4
8	d_o=0.65 cm B=8.4 kG	3.1	5.8	1.4	1.3	1.6	1.5
9		4.2	4.3	1.4	2.0	2.2	1.7
10	Vaned Cathode	9.7	5.5	2.9	3.0	2.5	1.6
11	d_o=1 cm B=6.6 kG	9.7	5.5	2.8	2.9	2.5	1.6
12		9.0	5.5	3.0	2.9	2.3	1.7
13		9.3	5.3	2.9	3.1	2.3	1.7

Table 1

NO.	CONFIGURATION	J_i (A/cm^2)	$\frac{J_i}{J_{ith}}$	$\frac{J_i}{J_{ic}}$	$\frac{J_i}{J_{ico}}$	γ $\frac{+100\%}{-36\%}$
1	Planar Cathode	30	0.5	0.7	2.2	1.3
		±15%	$\frac{+75\%}{-50\%}$	$\frac{+75\%}{-50\%}$	±25%	$\frac{+100\%}{-36\%}$
2	d_o=0.75 cm B=8.0 kG	43	0.8	1.1	3.5	1.3
3		40	0.7	1.0	4.4	1.4
4	Planar Cathode	46	1.0	1.5	4.7	1.3
5	d_o=0.75 cm B=6.7 kG	52	1.1	1.8	5.5	1.4
6		72	1.5	2.8	11.0	1.5
7	Planar Cathode	65	0.9	1.5	5.0	1.6
8	d_o=0.65 cm B=8.4 kG	65	1.1	1.4	4.8	2.4
9		80	2.1	2.4	8.2	3.9
10	Vaned Cathode	120	4.7	6.0	11	5.2
11	d_o=1 cm B=8.6 kG	120	4.6	5.8	11	4.6
12		120	5.0	6.0	11	5.2
13		120	5.5	6.6	12	4.8

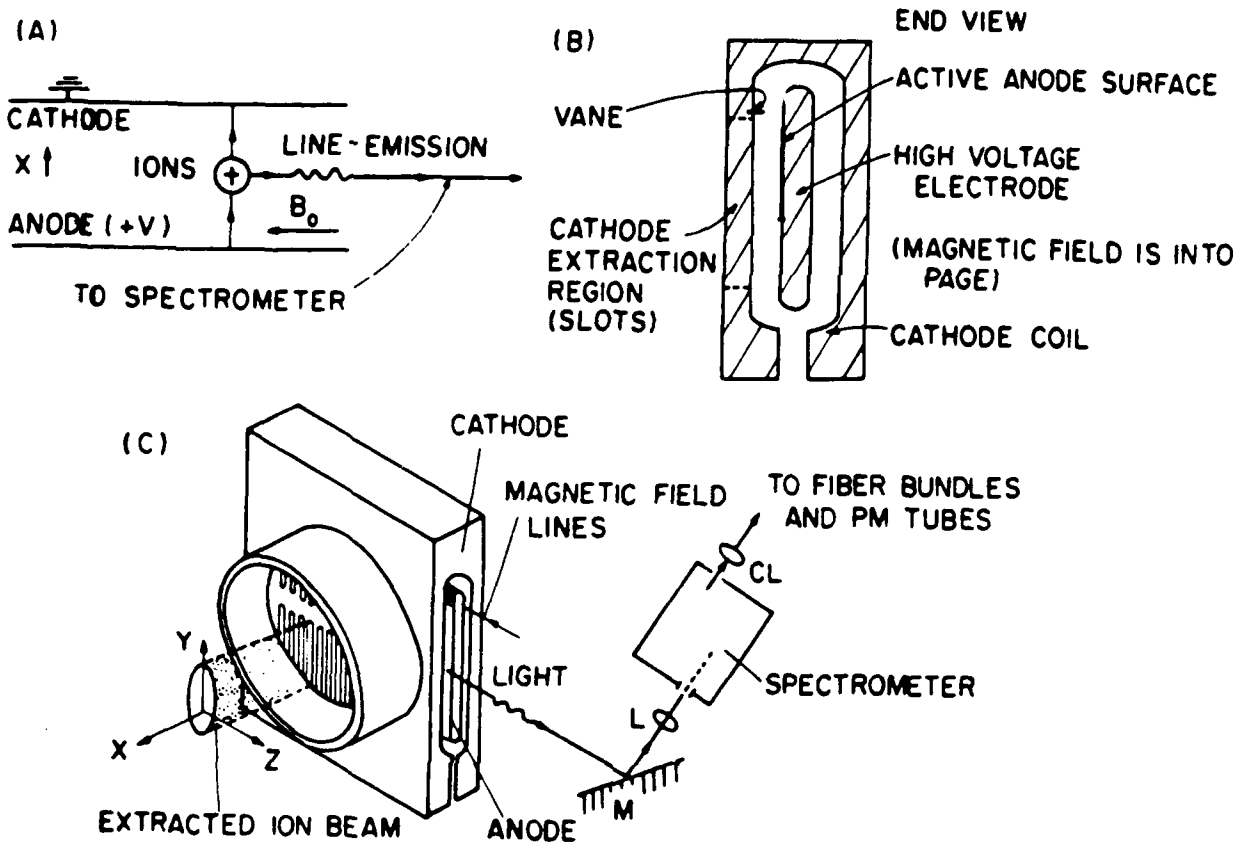

Fig. 1: (a) Method for measuring the electric field E in the acceleration gap of a magnetically insulated diode. (b) An end view of the ion diode showing the location of the cathode vane and the anode ion emission region. (c) Schematic illustration of the planar magnetically insulated ion diode and the optical arrangement. The distance of the observation region from the anode is varied by moving the mirror M in the x direction.

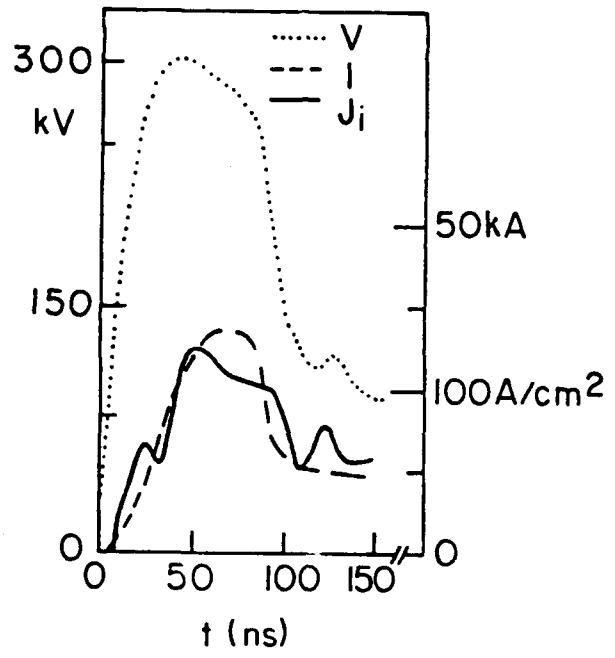

Fig. 2: Typical inductively corrected diode voltage (monitored by a capacitive probe) and diode current waveforms.

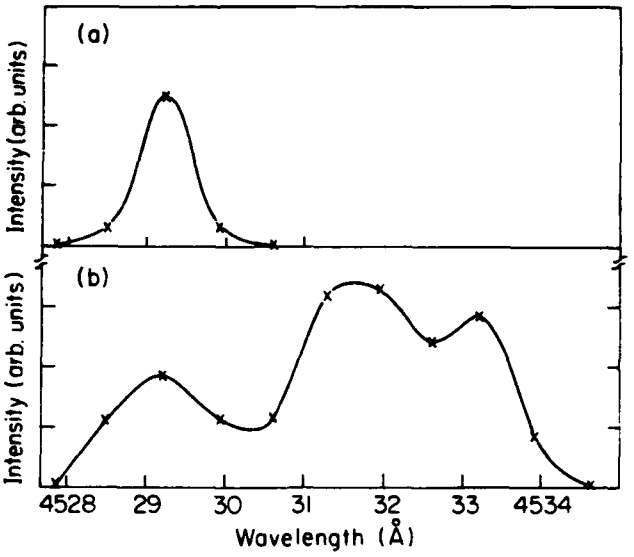

Fig. 3: (a) Spectral profile of the $4d_{5/2} \rightarrow 4p_{3/2}$ Al^{++} emission from the anode plasma (x=0.15 cm) at t=70 ns. The zero-field wavelength is 4529.2 Å. The initial A-K gap (d_o) was 0.65 cm, the peak diode voltage was about 300 kV, and B was 8.4kG. The spectral window of each fiber channel was 0.67 Å. (b) Profile of the emission from the acceleration gap: x=0.375 cm and t=65 ns. The lines in (a) and (b) indicate the trend.

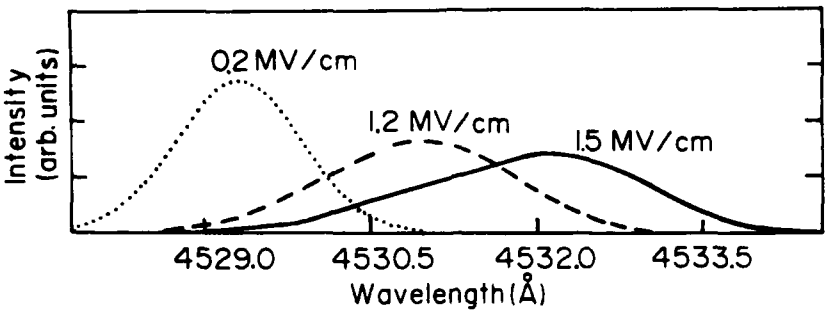

Fig. 4: Calculated spectral profiles for the $4d_{5/2} \rightarrow 4p_{3/2}$ Al^{++} emission for three electric fields with B=0. Each of the components of the shifted emission was assumed to be Gaussian-like with a FWHM of 1.3 Å due to Doppler broadening. The zero-field wavelength is 4529.2 Å.

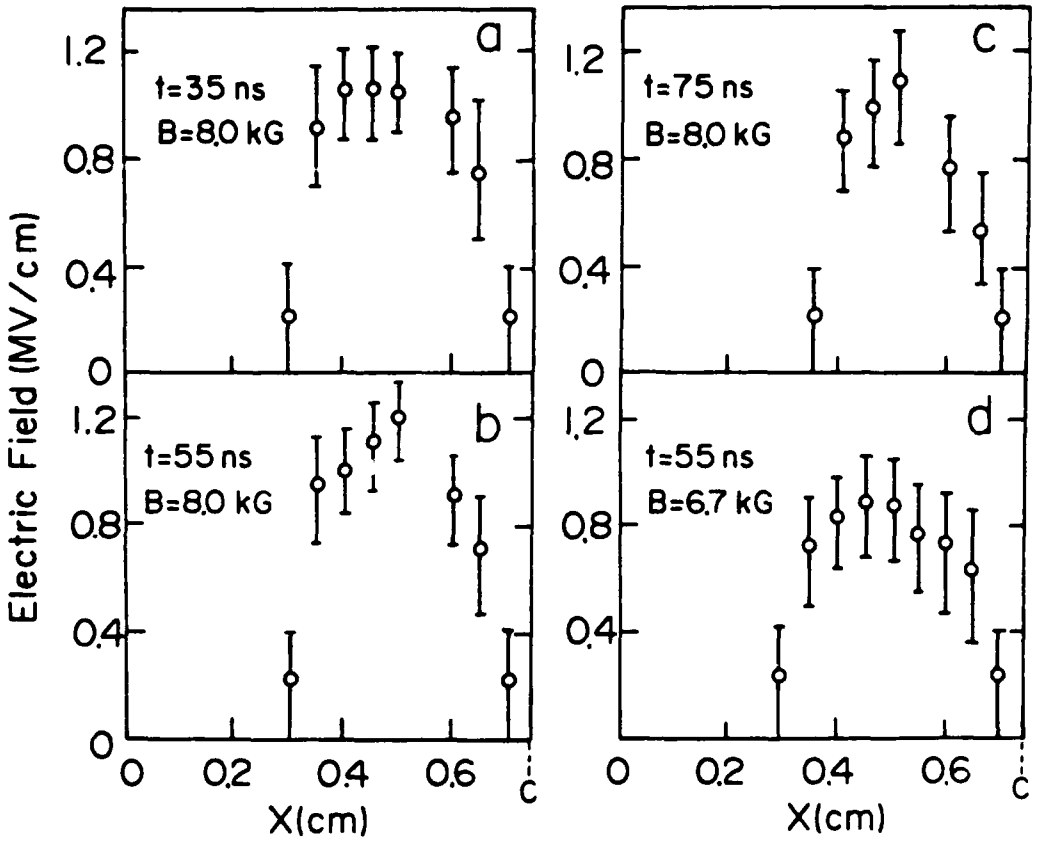

Fig. 5: The measured electric field distribution $E(x)$ for a planar diode configuration with d_o=0.75 cm is shown at the three times 35, 55, and 75 ns in (a), (b), and (c) respectively. (d) The electric field profile for a similar configuration but with a different applied magnetic field B. The solid anode surface is at x=0 and the cathode surface is indicated by C. Each point is an average of two discharges.

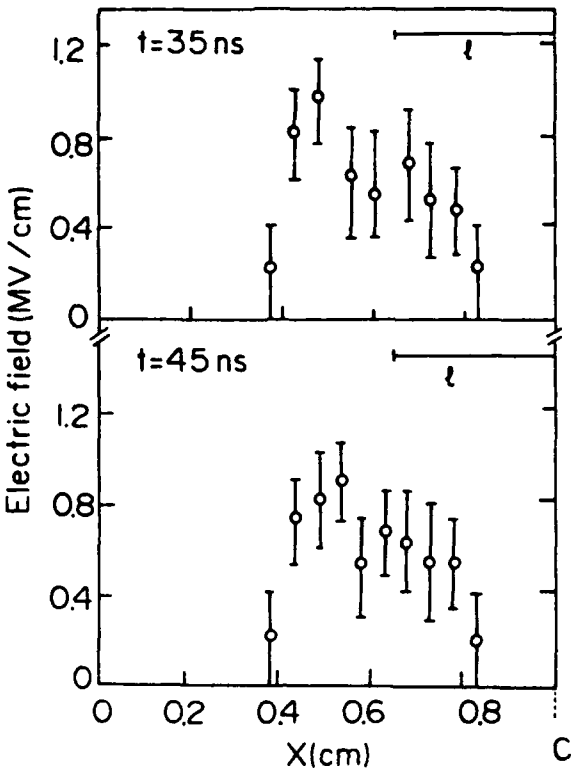

Fig. 6: Measured $E(x)$ profiles at two times for a vaned-cathode configuration with d_o=1cm, peak diode voltage about 280 kV, and B=6.6 kG. The solid anode surface is at x=0 and the cathode is indicated by C. Each point is an average of two discharges. The vane projected 0.35 cm off the cathode surface, as indicated by the line l.

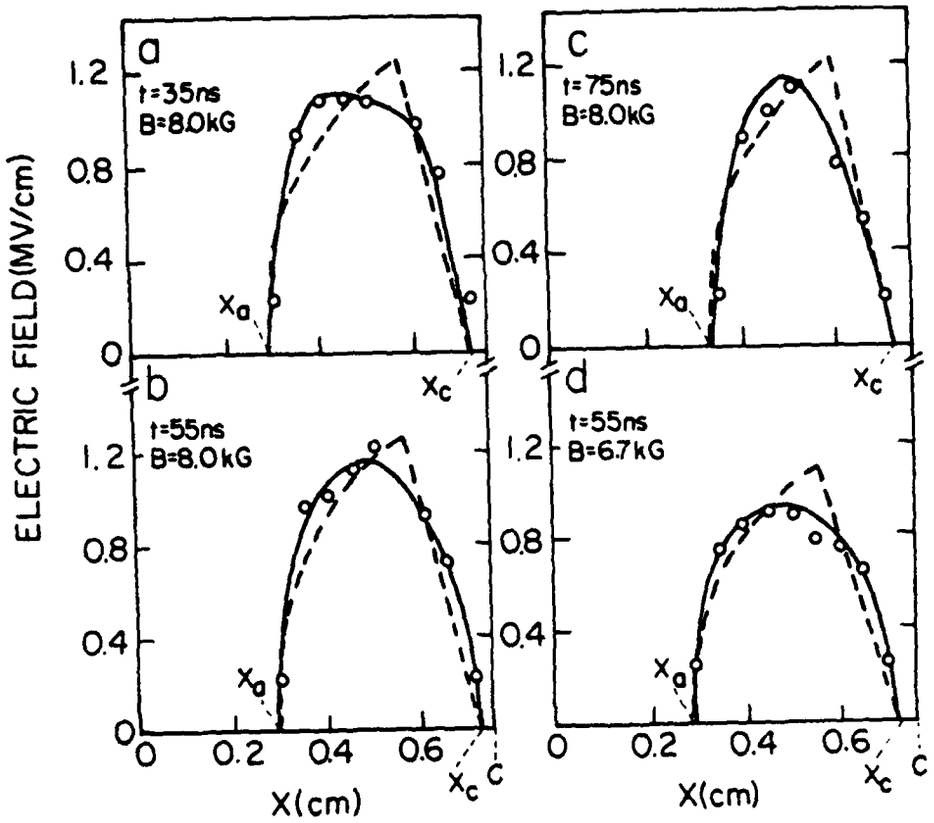

Fig. 7: The solid lines in (a), (b), (c), and (d) are simply smooth curves drawn through the data points (open circles) from Figs. 5 (a), (b), (c), and (d), respectively. The dashed lines are calculated[9] $E(x)$ profiles (see Sec. VA) using the instantaneous diode gap $d = x_c - x_a$, where x_a and x_c are the zero-field points on the anode and cathode sides, respectively.

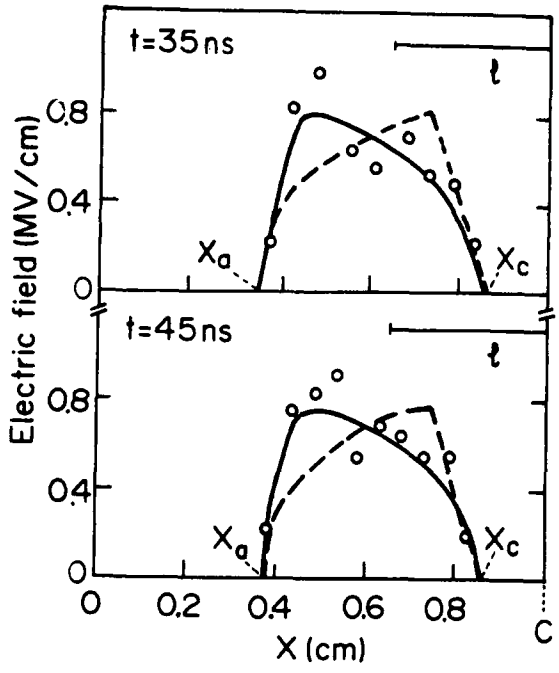

Fig. 8: The same as Fig. 7 but for the data in Fig. 6 (vaned configuration).

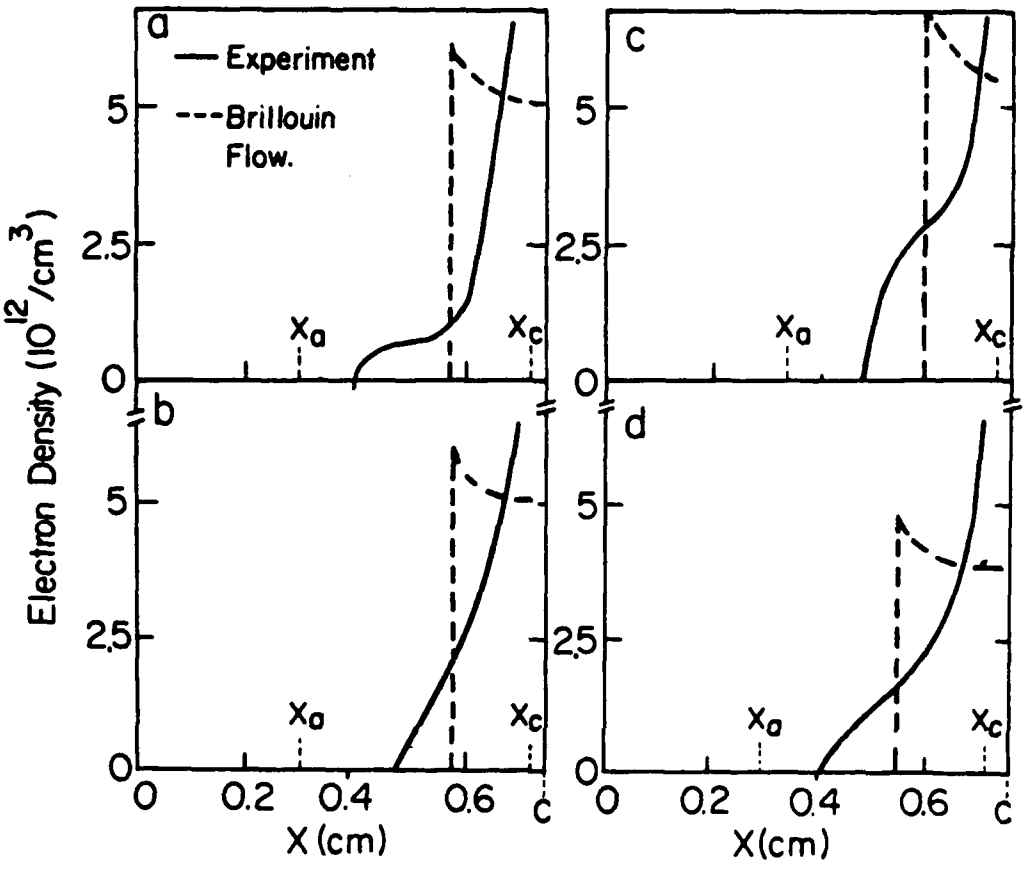

Fig. 9: Electron density profiles $n_e(x)$ inferred from the $E(x)$ profiles in Fig. 7. Also shown are the corresponding Brillouin-flow[9] profiles calculated using the actual diode gap d.

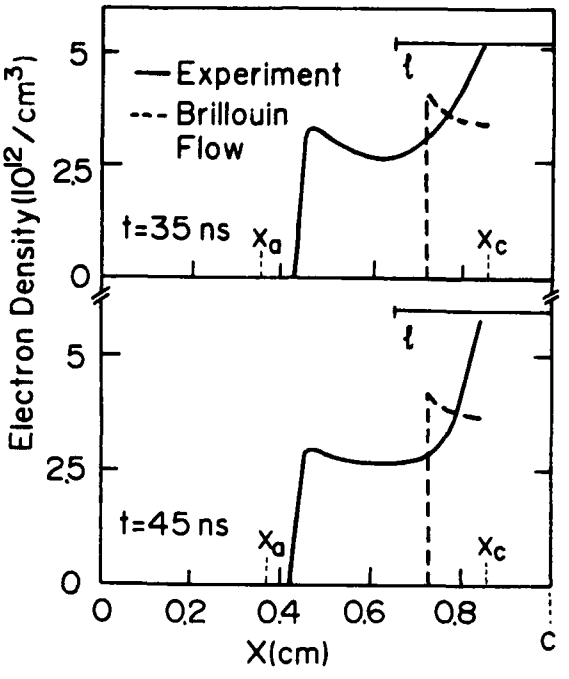

Fig. 10: Electron density profiles inferred from the $E(x)$ profiles in Fig. 8 and the corresponding Brillouin-flow[9] profiles.

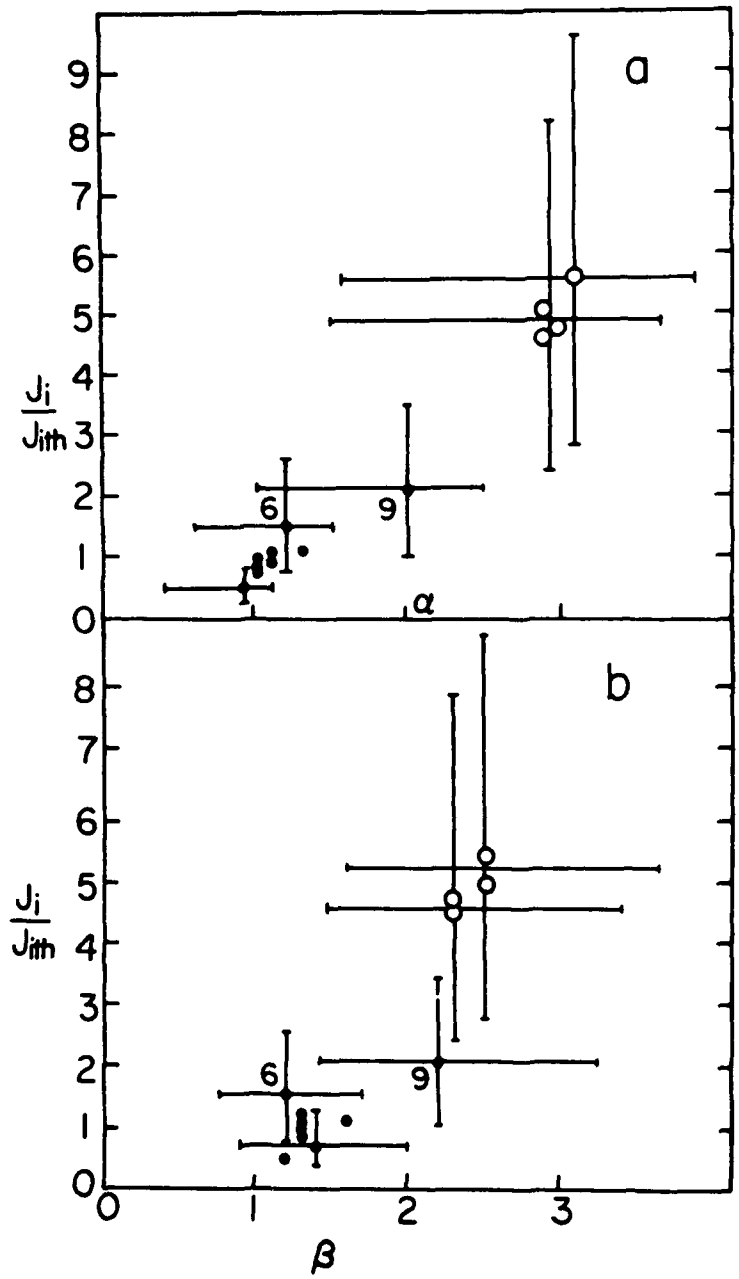

Fig. 11: The ion current density enhancement J_i/J_{ith} (with J_{ith} calculated[9] using the actual diode gap d) as a function of α and β for the cases listed in Table I. The circles belong to rows 10-13 (vaned-cathode configuration). The points marked by 6 and 9 correspond to rows 6 and 9 in Table I, respectively.

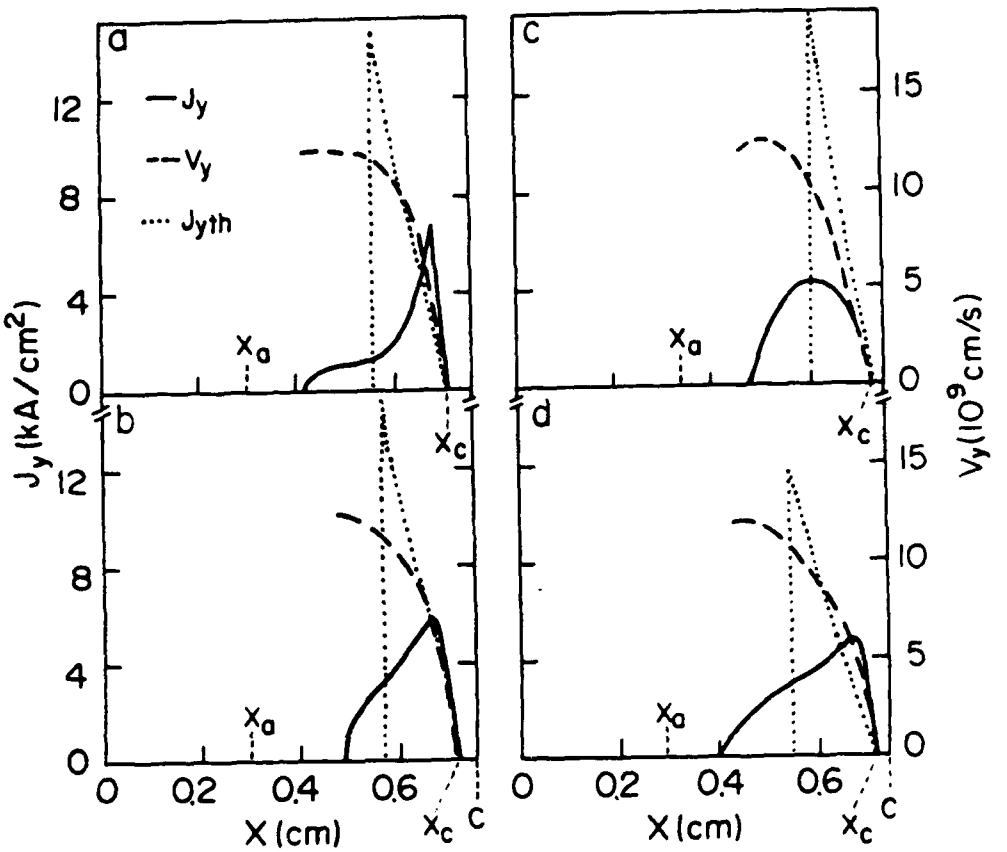

Fig. 12: Profiles of the electron drift velocity $| V_y(x) |$ and the drift current density $J_y(x)$ inferred from the $E(x)$ profiles in Fig. 7. Also shown are the corresponding theoretical[6] current densities $J_{yth}(x)$.

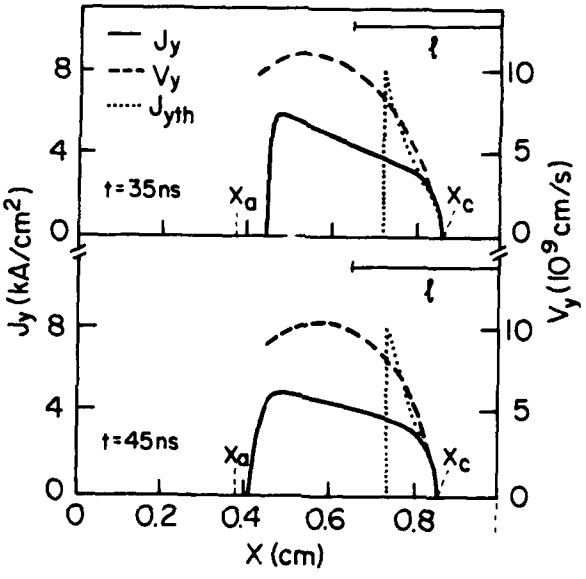

Fig. 13: Profiles of $\mid V_y(x) \mid$, $J_y(x)$, and $J_{yth}(x)$ for the cases in Fig. 8.

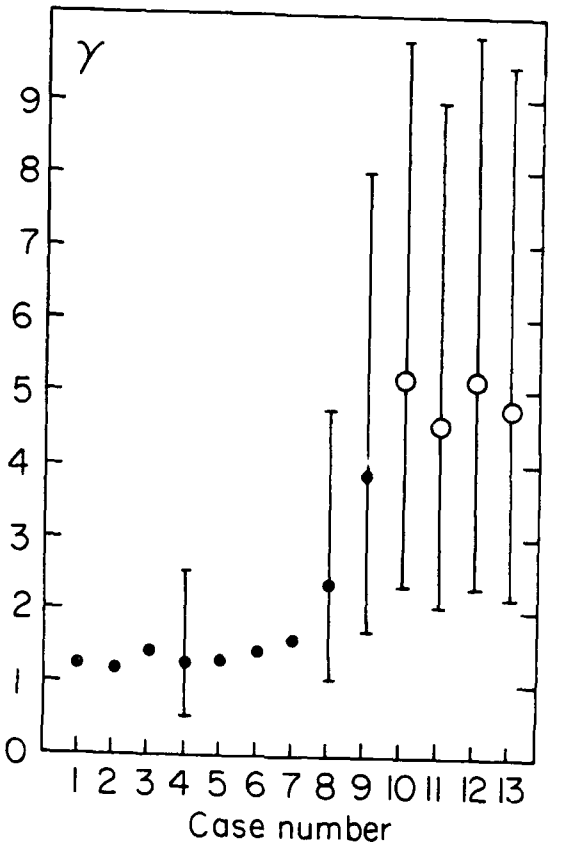

Fig. 14: The ratio $\gamma = I_y/I_{y_s}$ for the cases listed in Table I. The numbers along the ordinate are the row numbers in the table. The circles correspond to rows 10-13 in Table I (vaned configuration).

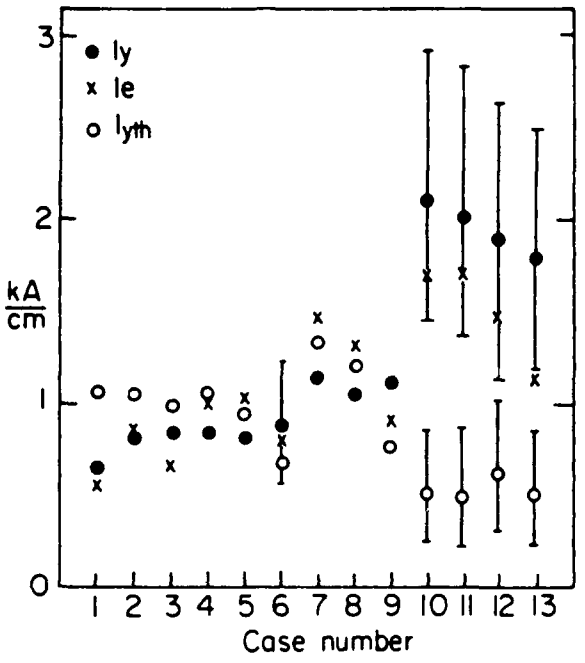

Fig. 15: The total electron drift current I_y obtained from integration of $J_y(x)$ and the corresponding calculated total drift current I_{yth} for the cases listed in Table I. Also shown is the diode electron current I_e per unit anode length.